# Interaction of O vacancies and domain structures in single crystal $BaTiO_3$: Two-dimensional ferroelectric model

L. Hong and A. K. Soh*
*Department of Mechanical Engineering, The University of Hong Kong, Hong Kong, China*

Q. G. Du and J. Y. Li
*Department of Mechanical Engineering, University of Washington, Seattle, Washington 98195-2600, USA*
(Received 5 December 2007; published 5 March 2008)

Two-dimensional simulations on the interactions of oxygen vacancies and different domain structures in barium titanate single crystal were carried out using the phase field method. The evolution of the spontaneous polarizations and oxygen vacancies was coupled through Maxwell's equation. The results showed that two barriers near the electrodes existed in both the 90° and 180° domain structures. It has also been observed that while an intrinsic electrostatic potential drop across the 90° domain wall created the electric fields which drove the electrons and oxygen vacancies aggregate on the different sides of the domain wall, the 180° domain wall had insignificant interaction with the potential, and no electron or vacancy accumulation in 180° domain structure was observed. Polarization charge density is believed to be the origin of this difference.

DOI: 10.1103/PhysRevB.77.094104 PACS number(s): 77.80.Dj, 73.40.−c, 61.72.jd

## I. INTRODUCTION

Oxygen vacancy is one of the common defects in ferroelectrics, and it is the most mobile one. The effects of oxygen vacancies on ferroelectrics can be modulated by adopting different oxidation processes[1] and donor dopants,[2] but cannot be eliminated. Therefore, it is very important to elucidate the working principles of oxygen vacancies in ferroelectrics properly, especially as the size of the functional ferroelectric devices is approaching nanoscale.

Many experiments have been carried out to study the influence of oxygen vacancy electromigration on different properties of ferroelectrics. For example, polarization fatigue phenomenon has been extensively studied to better understand how to improve the performance of ferroelectric thin film capacitors. Dearaujo *et al.*[3] pointed out that modification of either electrodes or ferroelectrics could hinder the fatigue process. Conductive oxides such as $IrO_2$, $RuO_2$, or $La_{0.7}Sr_{0.3}MnO_3$ (Refs. 3–5) have been testified to be superior than platinum electrodes due to their capacity to absorb oxygen vacancies on the interfaces of the electrodes and ferroelectrics. Doping $Pb(Zr_{0.52}Ti_{0.48})O_3$ thin films with Sr and Ba can effectively decrease the oxygen vacancy density and, thus, enhance the polarization fatigue endurance.[6] Moreover, the spontaneous normal-relaxor transition due to oxygen vacancy has also been observed.[7] Recently, Garcia *et al.*[8] found that the unexpected dielectric response around room temperature was related to the presence of oxygen vacancies.

Based on the experimental results, some theoretical and numerical models have been developed to study the migration and distribution of oxygen vacancies in ferroelectrics, and special attention has been paid to the relation between oxygen vacancies and domain walls. Scott and Dawber[9] have proposed a fatigue model to illustrate the oxygen vacancy ordering plane near the ferroelectric-electrode interface, which could effectively pin domain walls. He and Vanderbilt[10] performed a first-principles study on the interaction of oxygen vacancies and 180° domain walls and concluded that the formation energy for vacancies in the domain walls was lower than that in the bulk. As the oxygen vacancies are ionized, the electric potential in ferroelectrics should have the dominant effect on the migration of the vacancies. A small offset of electrostatic potential across the 90° domain wall in $PbTiO_3$ was first detected by Meyer and Vanderbilt[11] using the first-principles approach. Zhang and Goddard[12] have also found an electric potential across the two sides of a 90° domain wall. However, literature on the interaction of oxygen vacancies and domain structures in ferroelectrics subjected to an electric field is hardly available except the studies carried out by Xiao and co-workers[13] and Du[14].

In the present study, barium titanate $BaTiO_3$ (BTO) is considered as *n*-type semiconductor[15] where the oxygen vacancies act as single donors. A two-dimensional ferroelectric model is devised, based on the Ginzburg–Landau theory and the evolution of defects through diffusion,[13,14] to demonstrate the interactions between oxygen vacancies and the 90° and 180° domain walls, as well as the influence of electrostatic potential on the redistribution of vacancies. The proposed phase field model is implemented with proper boundary conditions and solved by Fourier and finite difference methods. The results show that the oxygen vacancies and the electrons are attracted into the different sides of 90° domain wall which is induced by the significant electric field inside it. However, the electrostatic potential and the distribution of oxygen vacancies in 180° domain walls are very different from those of the 90° domain walls due to the lack of potential drop across 180° domain walls. This model provides an approach to simulate the mesoscopic phenomena of ferroelectrics, but not the atomic scale phenomena, such as the influence of the vacancy diffusion on crystal lattice structure.

## II. SIMULATION METHODOLOGY

### A. Phase field model

A model is devised to study the electrode-ferroelectric-electrode geometry capacitor, where platinum electrodes on

 

the top and bottom are shorted. The effects of mismatch and the depolarizing field have significant influence on the polarization of ultrathin ferroelectric films, which is, however, not the case in this study; therefore, these two effects are not accounted for.

In the present simulation, a cubic-tetragonal transformation system is modeled. The total energy of the system is given by $F=F_L+F_G+F_{ela}+F_{electro}=\int_V[f_L+f_G+f_{ela}+f_{electro}]dV$, where $F_L$, $F_G$, $F_{ela}$, and $F_{electro}$ are the bulk-free energy, the gradient energy, the elastic strain energy, and the electrostatic energy, respectively. Note that the external electric field is not considered in this study.

The bulk-free energy density of ferroelectric BTO is described as follows:

$$\begin{aligned} f_L(P_i) = {} & \alpha_1(P_1^2+P_2^2+P_3^2)+\alpha_{11}(P_1^4+P_2^4+P_3^4) \\ & +\alpha_{12}(P_1^2P_2^2+P_2^2P_3^2+P_3^2P_1^2)+\alpha_{111}(P_1^6+P_2^6+P_3^6) \\ & +\alpha_{112}[P_1^4(P_2^2+P_3^2)+P_2^4(P_1^2+P_3^2)+P_3^4(P_1^2+P_2^2)] \\ & +\alpha_{123}(P_1^2P_2^2P_3^2), \end{aligned} \tag{1}$$

where $\mathbf{P}=(P_1,P_2,P_3)$ is the polarization vector and $i=1,2,3$ represents $x$, $y$, and $z$ axes, respectively. $\alpha_1$ and $\alpha_{11}$ are the temperature dependent dielectric stiffness; $\alpha_{12}$, $\alpha_{111}$, $\alpha_{112}$, and $\alpha_{123}$ are temperature independent higher order dielectric stiffness constants.

The spontaneous polarization gradient energy density in Ginzburg–Landau theory represents the domain wall energy density, which dominates the domain pattern, and the lowest order is given by

$$\begin{aligned} f_G(P_{i,j}) = {} & \frac{1}{2}G_{11}(P_{1,1}^2+P_{2,2}^2+P_{3,3}^2) \\ & +G_{12}(P_{1,1}P_{2,2}+P_{2,2}P_{3,3}+P_{3,3}P_{1,1}) \\ & +\frac{1}{2}G_{44}[(P_{1,2}+P_{2,1})^2+(P_{2,3}+P_{3,2})^2 \\ & +(P_{1,3}+P_{3,1})^2]+\frac{1}{2}G'_{44}[(P_{1,2}+P_{2,1})^2 \\ & +(P_{2,3}+P_{3,2})^2+(P_{1,3}+P_{3,1})^2], \end{aligned} \tag{2}$$

where $G_{11}$, $G_{12}$, $G_{44}$, and $G'_{44}$ are the gradient energy coefficients and the commas in the subscripts denote spatial differentiation.

For perovskite ferroelectric materials, the spontaneous polarization $P_i$ and spontaneous strain $\varepsilon_{ij}^0$ are generated during the change of crystal structure from cubic to tetragonal, and their relationships are as follows:

$$\begin{aligned} & \varepsilon_{11}^0 = Q_{11}P_1^2+Q_{12}(P_2^2+P_3^2), \quad \varepsilon_{13}^0 = Q_{44}P_1P_3, \\ & \varepsilon_{22}^0 = Q_{11}P_2^2+Q_{12}(P_3^2+P_1^2), \quad \varepsilon_{23}^0 = Q_{44}P_2P_3, \\ & \varepsilon_{33}^0 = Q_{11}P_3^2+Q_{12}(P_1^2+P_2^2), \quad \varepsilon_{12}^0 = Q_{44}P_1P_2, \end{aligned} \tag{3}$$

where $Q_{11}$, $Q_{12}$, and $Q_{44}$ are the electrostrictive coefficients. The elastic energy density can be calculated using

$$f_{ela} = \frac{1}{2}c_{ijkl}e_{ij}e_{kl}, \tag{4}$$

where $c_{ijkl}$ is the elastic stiffness tensor; the elastic strain $e_{ij}=\varepsilon_{ij}-\varepsilon_{ij}^0$ in which $\varepsilon_{ij}$ is the total strain. The boundary condition to be implemented is stress control without clamping.

The electrostatic energy is to account for the long range interactions of spontaneous polarizations, which can be described as[16,17]

$$f_{electro} = -\frac{1}{2}(E_1P_1+E_2P_2+E_3P_3), \tag{5}$$

where $E_1$, $E_2$, and $E_3$ are the electrostatic fields along the $x$, $y$, and $z$ axes, respectively. The electrostatic field is the negative gradient of the electrostatic potential $\phi$ induced by the spontaneous polarizations and the space-charge density ($\rho$) in the ferroelectrics, i.e., $E_i=-\phi_{,i}$. Maxwell's equation is employed to obtain the solution of the electrostatic potential as follows:

$$\nabla\cdot(-\varepsilon_0\nabla\phi+\mathbf{P}) = \rho(\phi,N_d), \tag{6}$$

where $N_d=1\times10^{24}$ m$^{-3}$ is the defect density of BTO and $\varepsilon_0=8.85\times10^{-12}$ F m$^{-1}$ is the dielectric constant of the vacuum. $\rho(\phi,N_d)$ is calculated based on the electrons donated by the defects, the electrons in the conduction band, and the holes in the valence band,[13]

$$\begin{aligned} \rho(\phi,N_d) = {} & ezN_d\left(1-\left[1+\frac{1}{g}\exp\left(\frac{E_d-e\phi-E_{Fm}}{K_BT}\right)\right]^{-1}\right) \\ & -eN_cF_{1/2}\left(\frac{E_{Fm}-E_c+e\phi}{K_BT}\right) \\ & +eN_vF_{1/2}\left(\frac{E_v-E_{Fm}-e\phi}{K_BT}\right), \end{aligned} \tag{7}$$

where $N_c$ and $N_v$ are the effective density of states in the conduction and valence bands, respectively, $E_{Fm}$ is the Fermi level of the electrode, which is equal to the Fermi level of a semiconductor in contact with a metal, $E_d$, $E_c$, and $E_v$ are the donor level, the conduction, and valence band edge energies of BTO, respectively, $F_{1/2}$ is the Dirac–Fermi integral, $K_B$ and $T$ are the Boltzmann constant and absolute temperature, respectively, and $z$ and $g$ represent the donor valency and the ground state degeneracy of the donor impurity level, respectively. The values of these parameters related to the space-charge density are listed in Ref. 18. Maxwell's equation couples the evolution of polarization and diffusion of oxygen vacancies. The finite difference method is used to obtain the electrostatic potential by iteration, and $10^{-5}$ is adopted as the required precision. The boundary conditions of electrostatic potentials implemented are top and bottom boundaries shorted and no flux exists at either the left or right side.

The evolution of the spontaneous polarization and oxygen vacancy are controlled through two equations as described below. The time and spatial dependent spontaneous polarizations are governed by the time dependent Ginzburg–Landau equation,

TABLE I. The normalized parameters used in the simulation.

| $\alpha_1^*$ | $\alpha_{11}^*$ | $\alpha_{12}^*$ | $\alpha_{111}^*$ | $\alpha_{112}^*$ | $Q_{11}^*$ | $Q_{12}^*$ | $Q_{44}^*$ | $c_{11}^*$ | $c_{12}^*$ | $c_{44}^*$ | $G_{11}^*$ | $G_{12}^*$ | $G_{44}^*$ | $G'^*_{44}$ |
|---|---|---|---|---|---|---|---|---|---|---|---|---|---|---|
| −1 | −1.31 | 1.21 | 1.1 | 0.48 | 0.0074 | −0.0029 | 0.004 | 94750 | 45696 | 58416 | 1.6 | 0.0 | 0.8 | 0.8 |

$$\frac{\partial P_i(\mathbf{r},t)}{\partial t} = -L\frac{\delta F}{\delta P_i(\mathbf{r},t)} \quad (i=1,2,3), \tag{8}$$

where $\mathbf{r}$ denotes spatial vector. In addition, $t$ and $L$ represent time and kinetic coefficients, respectively. The density of defects can evolve through diffusion,[13,14]

$$\frac{\partial N_d}{\partial t} = \nabla \cdot \left[ \beta N_d \nabla \left( \frac{\partial W_d}{\partial N_d} + ez\phi \right) \right], \tag{9}$$

where $\beta$ is the mobility and $W_d$ is the contribution to the free energy due to defects, which is assumed to be the usual free energy of mixing at small concentrations.

### B. Numerical implementation and simulation parameters

Fourier and finite difference methods are used to study the proposed phase field model. The evolution of polarization is investigated using Fourier method, and the mechanical equilibrium equation is solved using Green's function and Fourier method. In addition, Maxwell's equation and the diffusion equation of the vacancies are solved using the finite difference method.

Barium titanate is chosen for the present simulation. The material constants of the bulk-free energy and the electrostrictive coefficients are[19]

$$\alpha_1 = 3.3 \times (T-110) \times 10^5, \quad \alpha_{11} = 3.6 \times (T-175) \times 10^6, \quad \alpha_{12} = 4.9 \times 10^8, \quad \alpha_{111} = 6.6 \times 10^9,$$

$$\alpha_{112} = 2.9 \times 10^9, \quad \alpha_{123} = -2.5 \times 10^9, \quad Q_{11} = 0.11,$$

$$Q_{12} = -0.043, \quad Q_{44} = 0.059,$$

$$c_{11} = 1.755 \times 10^{11}, \quad c_{12} = 8.464 \times 10^{10},$$

$$c_{44} = 1.082 \times 10^{11}.$$

The set of normalized variables and effective coefficients described in Ref. 20 are employed in the present study. $\mathbf{r}^*$, $t^*$, and $\mathbf{P}^*$ are the normalized distance, time, and polarization, respectively. The others are the effective coefficients of the normalized variables,

$$\mathbf{r}^* = \sqrt{|\alpha_1|/G_{110}}\mathbf{r}, \quad t^* = |\alpha_1|Lt, \quad \mathbf{P}^* = \mathbf{P}/P_0,$$

$$\alpha_1^* = \alpha_1/|\alpha_1|, \quad \alpha_{11}^* = \alpha_{11}P_0^2/|\alpha_1|, \quad \alpha_{12}^* = \alpha_{12}P_0^2/|\alpha_1|,$$

$$\alpha_{111}^* = \alpha_{111}P_0^4/|\alpha_1|, \quad \alpha_{112}^* = \alpha_{112}P_0^4/|\alpha_1|, \quad \alpha_{123}^* = \alpha_{123}P_0^4/|\alpha_1|,$$

$$Q_{11}^* = Q_{11}P_0^2, \quad Q_{12}^* = Q_{12}P_0^2, \quad Q_{44}^* = Q_{44}P_0^2,$$

$$c_{11}^* = c_{11}/(|\alpha_1|P_0^2), \quad c_{12}^* = c_{12}/(|\alpha_1|P_0^2), \quad c_{44}^* = c_{44}/(|\alpha_1|P_0^2),$$

$$E^* = E/(|\alpha_1|P_0), \quad \varepsilon_0^* = \varepsilon_0|\alpha_1|,$$

$$G_{11}^* = G_{11}/G_{110}, \quad G_{12}^* = G_{12}/G_{110}, \quad G_{44}^* = G_{44}/G_{110},$$

$$G'^*_{44} = G'_{44}/G_{110}.$$

The Voigt shortened notations of the elastic stiffness tensors are used here. The normalized material coefficients are listed in Table I. The reference value of the gradient energy coefficients is $G_{110}=1\times10^{-7}$ C$^{-2}$ m$^4$ N and that of spontaneous polarization is $P_0=|\mathbf{P}_0|=0.26$ C m$^{-2}$. The value of $\alpha_1$ at 27 °C is $\alpha_0=\alpha_{1,27\,^\circ\mathrm{C}}=3.3\times(27-110)\times10^5$ C$^{-2}$ m$^2$ N. Thus, $l_0=\sqrt{G_{110}/|\alpha_0|}=60$ nm, $\rho_0=\sqrt{|\alpha_0|P_0^2/G_{110}}=0.43\times10^7$ C m$^{-3}$, and $\phi_0=\sqrt{G_{110}|\alpha_0|P_0^2}=0.43$ V. The normalized values of space-charge density and electrostatic potential are thus calculated as $\rho^*=\rho/\rho_0$ and $\phi^*=\phi/\phi_0$.

## III. SIMULATION RESULTS AND DISCUSSION

Two-dimensional simulations are carried out by employing $64\times64$ and $128\times64$ discrete grids for 90° and 180° domain structures, respectively. It is obvious that this phase field model can be extended to study the three-dimensional case. The grid spacing in real space is chosen to be $l_0$. Two shorted platinum electrodes are mounted on the top and bottom, and the periodic boundary conditions are implemented along the lateral direction. As the diffusion of oxygen vacancies in ferroelectrics is usually much slower than evolution of polarizations, the time steps of the polarization and diffusion of defects are set as 0.03 and 0.004, respectively, in order to obtain reasonable and convergent results.

### A. 90° domain structure

The initial periodic 90° domain structure is established using the same simulation procedure of the phase field method in Ref. 21. The pattern obtained is shown in Fig. 1.

Stating from the initial domain structure, the polarization and vacancies evolve simultaneously. The spontaneous polarization, the electrostatic potential, the charge density, and oxygen vacancies in BTO are stable after 1000 simulation steps. Figure 2 shows that the redistribution of the electrons and vacancies has little influence on the spontaneous polarizations. For the electrode-ferroelectric-electrode capacitor, the interfaces are widely accepted as Schottky barriers where the electric potential changes rapidly within the limited height, which can be seen in Fig. 2(b). The results show that the change of voltage of the barrier is about 1.3 V. Moreover, the electrostatic potential is periodically distributed with regular domain pattern in the body of BTO, and it decreases abruptly across the domain walls, thus creating significantly large electric fields within the domain walls, which

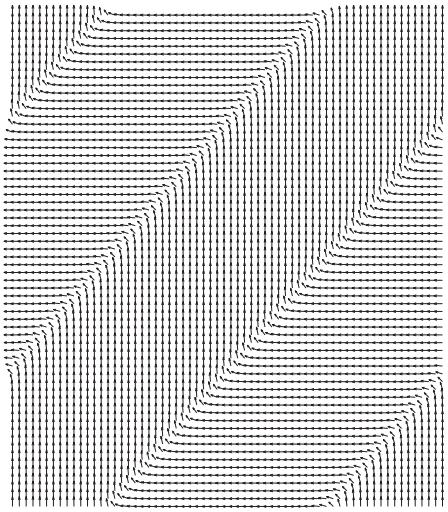

FIG. 1. Initial 90° domain pattern.

are shown in Fig. 3. The intrinsic potential distribution is directly resolved from Maxwell's equation, which demonstrates the important function of electrostatic potential in ferroelectric capacitors.

Due to the inhomogeneous distribution of the electrostatic potential, the electrons and oxygen vacancies also need to redistribute, as shown in Figs. 2(c) and 2(d). To start the diffusion process of oxygen vacancies, an initial random noise is applied. The results show that the oxygen vacancies and the electrons are attracted to the different sides of the domain walls because of the interior electric fields. This redistribution process is mainly taken place within the domain wall; thus, the densities of oxygen vacancies and charges in the domain itself do not change significantly. The accumulation of vacancies and electrons around the domain walls can be used to explain the domain wall pinning mechanism for polarization fatigue. In addition, the high density of electrons can also act as charge carrier if an electric field is applied, which will induce current leakage in the ferroelectric capacitors. The electrons and vacancies inside the Schottky barriers will migrate into electrodes, and the former will diffuse faster than the latter. The final mean value of oxygen vacancies is about 2.7% smaller than the initial one. If the initial polarization is reversed, the distributions of the electrostatic potential, charge, and oxygen vacancy densities would show a mirrorlike reverse effect.

The one dimensional distributions of electrostatic potential, electric field, and oxygen vacancy along the middle line of the 90° domain pattern are plotted in Fig. 3. There is a 0.45 V voltage drop between the two sides of the domain wall, which is comparable with other predicted values of 0.18 V in Mayer and Vanderbilt,[11] 0.115 V in Xiao and co-workers,[13] and 0.23 V in Zhang and Goddard.[12] Consequently, a maximum electric field of 3.5 MV/m is produced inside the 90° domain wall, driving the redistribution of electrons and vacancies. Such magnificent electric field has also been found through the quantum mechanics calculations.[12] It is obvious that the oxygen vacancies in the body of the domain only diffuse slightly; however, those around the domain walls are pulled out of one side and diffused into the other side.

### B. 180° domain structure

First of all, an 180° domain structure with gradual polarization change across the domain wall is manually estab-

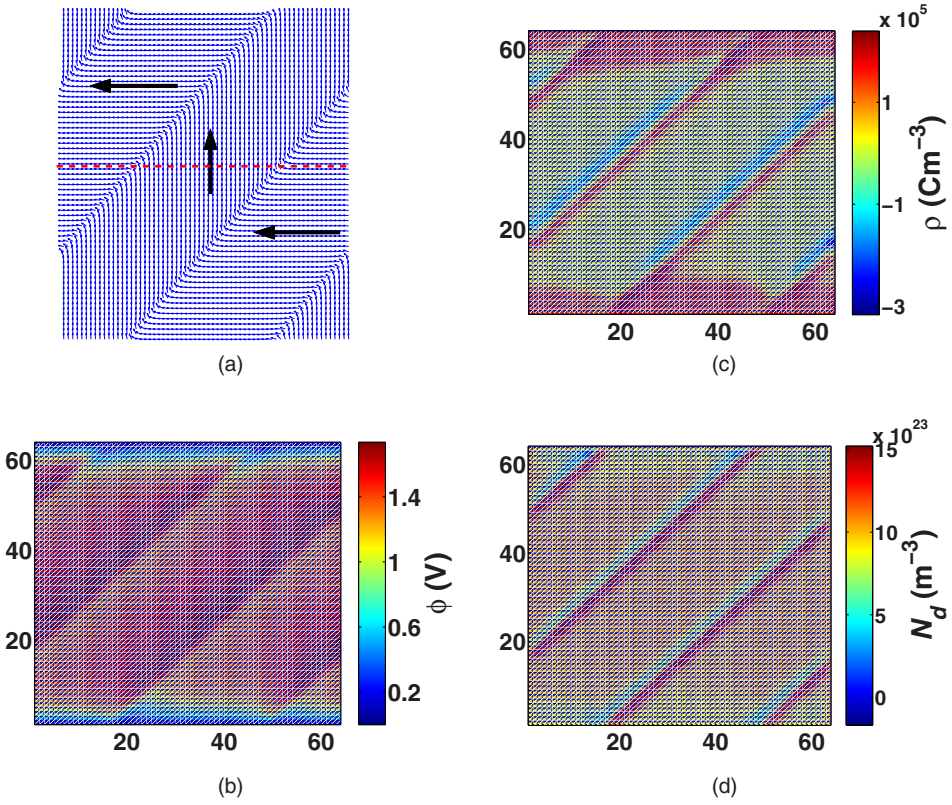


FIG. 2. (Color online) The distribution of (a) spontaneous polarization, (b) electrostatic potential, (c) charge density, and (d) oxygen vacancy density in 90° domain structure.

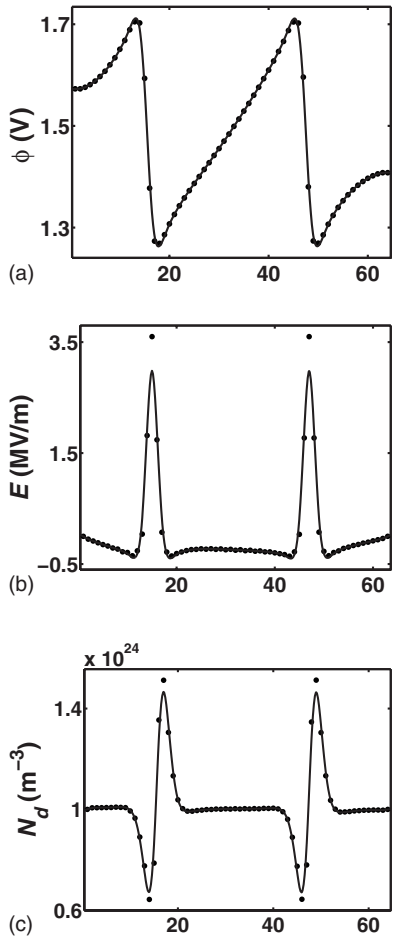


FIG. 3. The (a) electrostatic potential, (b) electric field, and (c) oxygen vacancy distribution along the red dashed line in the middle of the domain model in Fig. 2. Dots represent the calculation values and the solid lines are the fitting results.

lished (not shown here). This domain structure is subsequently evolved into a perfect one with sharp domain wall [Fig. 4(a)]. Two Schottky barriers exist on the upper and lower interfaces, and the electrons and vacancies are partly moved out of the two barriers, similar to the case of 90° domain structure. However, 180° domain wall has little influence on the electrostatic potential, which is obvious from the observation that the potential does not change and the electrons as well as vacancies do not aggregate around the domain wall. Based on these findings, we may infer that the 180° domain structure is preferable than 90° domain pattern for resisting polarization fatigue and leakage of donor doped ferroelectric capacitors.

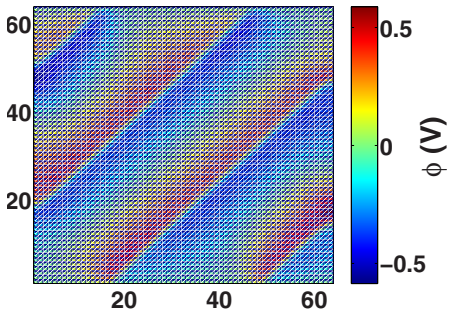


FIG. 5. (Color online) The electrostatic potential distribution of dielectric BTO in 90° domain structure.

### C. Two additional cases

For the sake of comparison, two additional simulation cases are carried out in which the same boundary conditions are implemented. In the first case BTO is treated as a perfect dielectric ferroelectric, which is traditionally without electrons and oxygen vacancies, thus space-charge density $\rho=0$. Figure 5 shows that the dielectric BTO also possesses the intrinsic potential change in the 90° domain walls induced by the polarization charge density, which provides the original driving force to attract the possible electrons or ionized defects. However, the electrostatic potential of BTO with 180° domain structure varies very slightly across the whole body (not shown). Therefore, it is reasonable to regard 90° domain walls as the seed of problem creations.

In the other case, immobile oxygen vacancies with $N_d = 1 \times 10^{24}$ m$^{-3}$ is considered. The electrostatic potential distributions of the two domain structures are kept the same to

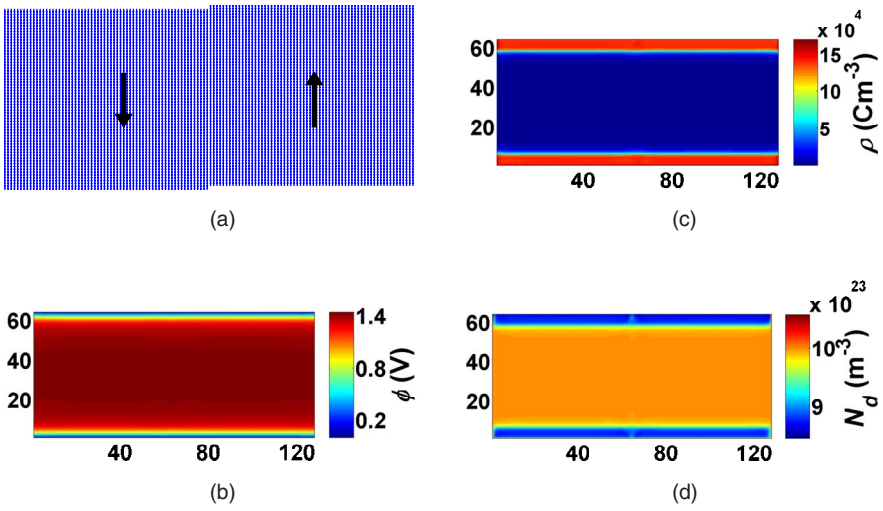


FIG. 4. (Color online) The distribution of (a) spontaneous polarization, (b) electrostatic potential, (c) charge density, and (d) oxygen vacancy density in 180° domain structure.

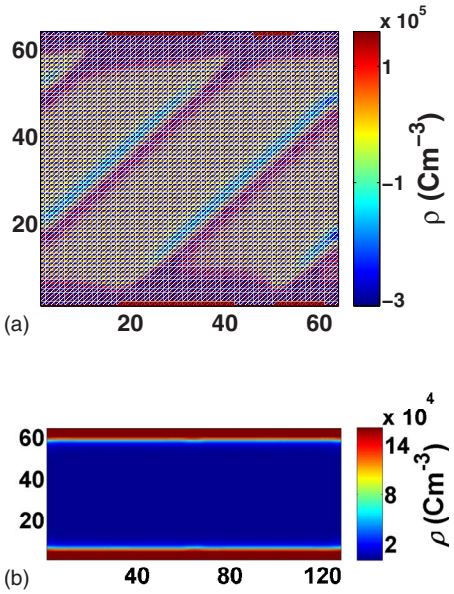


FIG. 6. (Color online) The charge density distributions of (a) 90° and (b) 180° domain structures in the case of immobile oxygen vacancies considered.

those with the case of mobile vacancies. The distributions of the charge density (Fig. 6) demonstrate that electrons are depleted in all the Schottky barriers, and the electric fields inside 90° domain walls drive the electrons to a concentrated region. Combined with the results of mobile oxygen vacancies, the aggregation of electrons and vacancies on the two sides of 90° domain walls is mainly induced by the magnificent electric field inside the domain walls. Note that the charge density distribution is also unaffected by the 180° domain wall.

The different electrostatic potential distributions in the 90° and 180° domain walls are due to different polarization charge density arrays in different domain wall structures. For the head-to-tail 90° domain wall, there exist positive and negative polarization charge planes on the two sides of the domain wall intrinsically, which induce a potential drop regardless of the inclusion of space charges. In contrast, the positive and negative polarization charges distribute equally on each side of the 180° domain wall, where no potential difference appears even though spacecharges are considered.

## IV. CONCLUSION

The relationship between oxygen vacancies and domain walls has been studied using the phase field method. Two barriers with depleted electrons emerge near the electrodes. Moreover, there is an intrinsic electrostatic potential drop across a 90° domain wall regardless of the consideration of BTO as *n*-type semiconductor or dielectric. This voltage change creates a large electric field, which promotes the asymmetric charge distribution around 90° domain wall, where electrons and oxygen vacancies concentrate on the opposite sides. Thus, polarization fatigue and leakage of ferroelectric capacitors are possibly originating from 90° domain walls, whereas 180° domain walls have insignificant interaction with the potential, and there is no electron or vacancy accumulation in this domain structure. The different interactions between vacancies and domain walls are induced by the intrinsically different polarization charge density arrays in different domain wall structures. Therefore, this study illustrates the origin and results of different interactions between vacancies and domain walls, which may provide ideas for experimental observations and computational simulations.

## ACKNOWLEDGMENT

Support from the Research Grants Council of the Hong Kong Special Administrative Region, China (Project No. HKU 716007E) is acknowledged. Q.G.D. and J.Y.L. acknowledge support from U.S. Army Research Office MURI Program (W911NF-07-1-0410).

*Author to whom correspondence should be addressed; FAX: +852 −28585415; aksoh@hkucc.hku.hk

[1] W. Li, A. P. Chen, X. M. Lu, and J. S. Zhu, J. Appl. Phys. **98**, 024109 (2005).
[2] Z. Zhang, L. Lu, C. Shu, and P. Wu, Appl. Phys. Lett. **89**, 152909 (2006).
[3] C. A. P. Dearaujo, J. D. Cuchiaro, L. D. Mcmillan, M. C. Scott, and J. F. Scott, Nature (London) **374**, 627 (1995).
[4] G. Asano, H. Morioka, and H. Funakubo, Appl. Phys. Lett. **83**, 5506 (2003).
[5] W. Wu, K. H. Wong, C. L. Choy, and Y. H. Zhang, Appl. Phys. Lett. **77**, 3441 (2000).
[6] Y. Wang, Q. Y. Shao, and J. M. Liu, Appl. Phys. Lett. **88**, 122902 (2006); Y. Wang, K. F. Wang, C. Zhu, T. Wei, J. S. Zhu, and J. M. Liu, J. Appl. Phys. **101**, 046104 (2007).
[7] G. Deng, G. Li, A. Ding, and Q. Yin, Appl. Phys. Lett. **87**, 192905 (2005).
[8] J. E. Garcia, V. Gomis, R. Perez, A. Albareda, and J. A. Eiras, Appl. Phys. Lett. **91**, 042902 (2007).
[9] M. Dawber and J. F. Scott, Appl. Phys. Lett. **76**, 1060 (2000); J. F. Scott and M. Dawber, *ibid.* **76**, 3801 (2000).
[10] L. He and D. Vanderbilt, Phys. Rev. B **68**, 134103 (2003).
[11] B. Meyer and D. Vanderbilt, Phys. Rev. B **65**, 104111 (2002).
[12] Q. Zhang and W. A. Goddard, Appl. Phys. Lett. **89**, 182903 (2006).
[13] Y. Xiao, Ph.D. thesis, Caltech University, 2005; Y. Xiao, V. B. Shenoy, and K. Bhattacharya, Phys. Rev. Lett. **95**, 247603 (2005).
[14] Q. G Du, Ph.D. thesis, University of Washington, 2007.
[15] J. F. Scott, *Ferroelectric Memories* (Springer, New York, 2000).
[16] Y. L. Li, S. Y. Hu, Z. K. Liu, and L. Q. Chen, Appl. Phys. Lett. **81**, 427 (2002).
[17] J. Wang and T. Y. Zhang, Phys. Rev. B **73**, 144107 (2006).

[18] The parameters to calculate space charges are from Ref. 13: $N_c$ and $N_v$ equal to $1\times10^{24}$ $m^{-3}$, $E_{Fm}$,$E_v$ and $E_c$,$E_d$ are −5.3, −4.0 eV and −3.6, −6.6 eV respectively, $z$ and $g$ equal to 1 and 2, respectively.

[19] N. A. Pertsev, A. G. Zembilgotov, and A. K. Tagantsev, Phys. Rev. Lett. **80**, 1988 (1998); N. A. Pertsev and H. Kohlstedt, arXiv:cond-mat/0603762v2 (unpublished).

[20] H. L. Hu, and L. Q. Chen, Mater. Sci. Eng., A **238**, 182 (1997).

[21] A. K. Soh, Y. C. Song, and Y. Ni, J. Am. Ceram. Soc. **89**, 652 (2006).